Optical Modeling of the Jefferson Laboratory IR Demo FEL

George R. Neil, Stephen V. Benson, Michelle D. Shinn, Paul C. Davidson, and Peter K. Kloeppel

Thomas Jefferson National Accelerator Facility (formerly CEBAF)
12000 Jefferson Avenue, Newport News, VA 23606

ABSTRACT

The Thomas Jefferson National Accelerator Facility (formerly known as CEBAF) has embarked on the construction of a 1 kW free-electron laser operating initially at 3 microns that is designed for laser-material interaction experiments and to explore the feasibility of scaling the system in power and wavelength for industrial and Navy defense applications. The accelerator system for this IR Demo includes a 10 MeV photocathode-based injector, a 32 MeV CEBAF-style superconducting radio-frequency linac, and single-pass transport which accelerates the beam from injector to wiggler, followed by energy-recovery deceleration to a dump. The electron and optical beam time structure in the design consists of a train of picosecond pulses at a 37.425 MHz pulse repetition rate. The initial optical configuration is a conventional near-concentric resonator with transmissive outcoupling. Future upgrades of the system will increase the power and shorten the operating wavelength, and utilize a more advanced resonator system capable of scaling to high powers. The optical system of the laser has been modeled using the GLAD® code by using a Beer's-law region to mimic the FEL interaction. Effects such as mirror heating have been calculated and compared with analytical treatments. The magnitude of the distortion for several materials and wavelengths has been estimated. The advantages as well as the limitations of this approach are discussed.

Keywords: free-electron laser (FEL), photocathode, injector, wavelength, optical, accelerator

1. INTRODUCTION

Thomas Jefferson National Accelerator Facility (Jefferson Lab) has recently received funding from the U.S. Department of the Navy, U.S. DOE, the Commonwealth of Virginia, and Industry to demonstrate high average power generation in a free-electron laser. The goal of the program is technology and application development of laser sources (on the order of 100 kW or higher) with high efficiency and low cost per photon, for defense and industrial applications. The first step in the program is to demonstrate kilowatt level average power in a FEL and to test out the technologies and physics required to scale the system to higher powers. Important technologies for high average power include energy recovery, superconducting RF (SRF) accelerators, multipass acceleration, and high-current injectors. We must also understand the physics of electron beam halo formation and emittance preservation.

The design wavelength for the Jefferson Lab FEL was chosen to be 3 μm with the plan to upgrade later to 1–2 μm and eventually 0.2 μm. Members of the Laser Processing Consortium, a group of industrial and university collaborators interested in exploring the potential uses of high power FELs in micromachining, polymer, and metal surface processing, plan to use the FEL at several wavelengths in the mid-infrared [1].

The accelerator and FEL hardware is scheduled to be complete and installed by Sept. 1997. This ambitious schedule necessitates the use of existing technology wherever possible. Experience, infrastructure, and designs developed in the construction and commissioning of the 4 GeV machine at Jefferson Lab and other accelerators will be used to reduce design and construction time.

Further author information -
G.R.N.: Email: neil@jlab.org; Telephone: 757-269-7443; S.V.B.: Email: felman@jlab.org; Telephone: 757-269-5026
M.D.S.: Email: shinn@jlab.org; Telephone: 757-269-7565; P.C.D.: Email: p.c.davidson@larc.nasa.gov; Telephone: 757-269-5849
P.K.K.: Email: kloeppel@jlab.org; Telephone: 757-269-7569

2. DESIGN OVERVIEW

The layout for the infrared demonstration FEL (IR Demo FEL) is shown in Figure 1. The electrons are produced in a 350–500 kV DC photocathode gun [2] and accelerated to 10 MeV in a superconducting accelerating unit with 1 meter of active length. The electrons are then accelerated in an SRF cryomodule up to an energy of 42 MeV. In order to minimize emittance-growth effects and to accelerate the commissioning process, the FEL is placed at the exit of the linac. The electron beam is deflected around two cavity mirrors in two magnetic chicanes with a path-length dispersion (M_{56}) of 30 cm. After the FEL, the beam can be recirculated for energy recovery and dumped at the injection energy of 10 MeV. The recirculation loop is based on the isochronous achromat used in the Bates accelerator [3] and is similar to the design presented in previous work [4]. Unlike the design in [4] however, this lattice has been designed with an energy acceptance of 6%.

Calculations indicate that emittance growth in the Bates 180° bend might be significant [5]. This growth poses problems for any future two-pass system. In order to predict future performance, we plan to carefully measure the emittance before and after the Bates bend and compare the results with calculations.

Table 1 summarizes the wiggler and accelerator parameters. We estimate, using parameterizations of the FEL equations [6], that the power output at 3 μm for these parameters should be 980 W with a small signal gain of 46%. Simulations of the entire acceleration process from the photocathode to the FEL using the code PARMELA predict transverse and longitudinal emittances approximately half of those listed in Table 1. If this beam performance is obtained and an rms wiggler parameter K of 1.0 is used, it should be straightforward to lase at the third harmonic (at 1.35 μm, the higher K resulting in fundamental lasing around 4 microns), with approximately one third the power at the fundamental and a gain of 48%. For the emittances in Table 1, the third harmonic gain is approximately 14%.
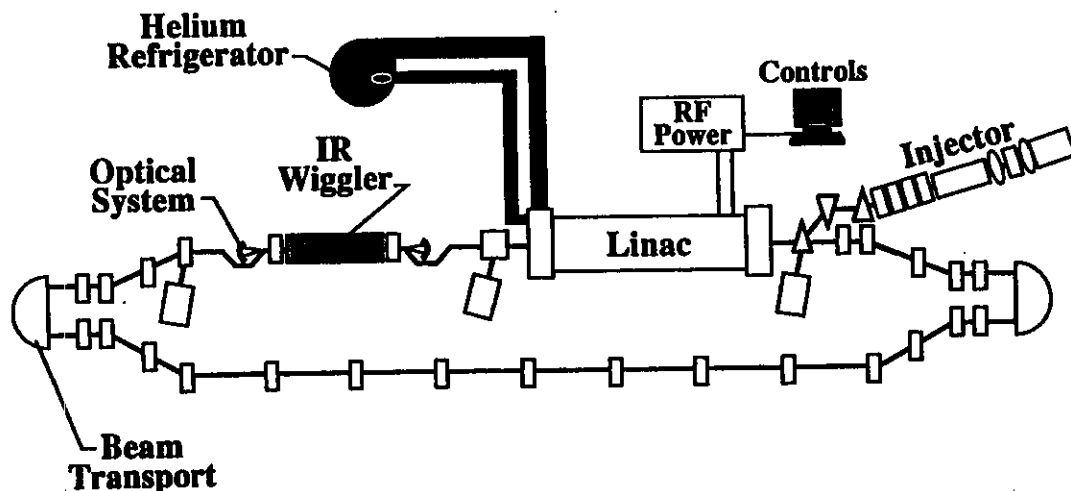

Figure 1. Layout of the IR Demo FEL. The electron beam is injected into the accelerator at 10 MeV, is accelerated to 42 MeV, goes through the FEL, is recirculated back to the linac, and is decelerated back down to 10 MeV and dumped.

Table 1. Parameters for the IR Demo FEL

Electron Beam Parameter		Wiggler	
Kinetic Energy	42 MeV	Period	2.7 cm
Average current	5 mA	Number of periods	40
Repetition rate	37.425 MHz	rms K^2	0.5 (optionally 1.0)
Charge per bunch	135 pC	Phase noise	$<5°$ rms
Norm. transverse emittance	13 mm-mrad	Trajectory wander	x $<\pm100$ μm y $<\pm500$ μrad
Longitudinal emittance	50 keV-deg		
β function at wiggler center	50 cm		
Energy spread (σ_γ/γ)	0.20%		
Peak current	50 A		
Bunch length (rms)	1 psec		

Reference [7] discusses the origin of the requirements for the optical resonator and discusses in detail the effects of mirror distortion on the resonator. In summary the specifications for the IR Demo resonator are as follows:

Table 2. Optical resonator requirements

Parameter	Requirement	Comments
Resonator type	Stable near-concentric	Best choice for low gain oscillator with small waist and large mode size on mirrors.
Center wavelength (λ)	3–4 μm	Compromise design wavelength determined from wiggler design with margin for lower energy.
Cavity length (L)	8.0105m	Compromise between mirror loading and tilt sensitivity
Rayleigh range (z_r)	40 cm	Nearly optimum for FEL gain.
Output coupling	13%	Provision must be made for larger and smaller values.
Length stability	0.5 μm rms	Passive control preferred.
Controls and diagnostics	Remotely controlled and read out.	Should also be computer interfaced.
Extraneous losses	<1% from all sources but output coupling.	Should be as low as possible.
Mirror tilt tolerance	2.6 μrad rms	This in a symmetric mode
Mirror radius	2.54 cm	Commercially available and larger than required for 7 μm operation
Mirror radius of curvature	4.045±0.008 m	Cold cavity tolerance

In addition to these laser requirements there are requirements for the optics as far as environmental effects are concerned. The accelerator tunnel is a relatively harsh environment with great quantities of ionizing radiation and the need for high vacuum mounting of the optical elements. Optics and mounting hardware must be compatible with ionizing radiation, and high vacuum. All controls must be remotely operated and all diagnostics must be remotely-monitored.

The IR Demo issue that is unique among existing FELs is mirror heating. The resulting distortions can potentially have effects on the lasing mode, the location of the cavity waist, and, if sufficiently severe, terminate the lasing process itself. It might also be anticipated that such distortion might affect the outcoupled optical beam quality but previous analysis Reference [8] has shown that by the time the distortion is severe enough to affect beam quality the power has been severely reduced. The analysis and modeling performed to predict the performance of the FEL in the presence of mirror heating is the subject of the remainder of this article.

3. MIRROR DISTORTION–ANALYTIC APPROACH

Since the mirrors use dielectric reflective coatings, the power absorbed in the coating should be a small fraction of the incident power but it is significant because of the high intracavity powers of the FEL. The total power absorption in the high reflector should be less than 10 W, and the distortion in the mirror can be made quite small by the use of an appropriate substrate. The substrate can be chosen to optimize the thermal characteristics of the mirror since the mirror need not be transparent. We will therefore assume initially that only the output coupler is distorted by mirror heating. Since the optical mode is cylindrically symmetric, the heating of the mirror will lead to a change in the effective radius of curvature of the mirror as well as producing spherical aberrations (assuming symmetric boundary conditions). Let us first consider the effects of the change in the mirror radius of curvature. Since only one mirror is distorted, the waist in the resonator will change in both size and position. Equation (10) in reference [7] gives the change in the Rayleigh range when both mirrors change their radii of curvature by the same amount. In this case, only one mirror changes and so the change in the Rayleigh range is only half as much or $M/4$ times the relative radius of curvature change where $M = 1 + (\frac{L}{2z_R})^2$. This statement sounds like an oversimplification but, in fact, the exact derivation of the change in Rayleigh range due to the change in curvature of one mirror yields a solution which is half of the value in equation (10). The change in the waist position with the radius of curvature of one mirror may be found by differentiating with respect to g_j ($\equiv 1 - \frac{L}{R_j}$ in conventional notation), multiplying by the derivative of g with respect to R and evaluating at $g_j = g_2$,

$$\Delta z = -\frac{L}{4g}\frac{\Delta R}{R} = \frac{LM}{4(M-2)}\frac{\Delta R}{R} \tag{1}$$

and we can calculate the change in the waist position and size from:

$$\frac{\Delta z_R}{z_R} = \frac{M}{4}\frac{\Delta R_c}{R_c} \text{ (for a change in one mirror's } R_c) \tag{2}$$

For large M the change in the waist position is just one quarter of the cavity length times the relative change in the radius of curvature. The sign is such that in increase in the radius of curvature will move the waist away from the mirror which is distorting.

As a numerical example, let us assume that the mirror radius of curvature changes by 1% due to heating, the cavity length is 8 m, and that the magnification $M=100$. The Rayleigh range will change by $0.01M/4$ or 25%. The waist position will change by one 400th of the cavity length which is 2 cm. Note that this change in the Rayleigh range will increase the intensity on the mirrors by 25% as well. The full effect on the cavity mode must be calculated self-consistently. The total effect can, in some circumstances, be much larger than the first order effect. As noted in reference [7], the gain will start to decrease rapidly if the Rayleigh range increases to over ~80 cm. One can therefore tolerate a total change of up to a factor of 100% if one starts with a Rayleigh range of 40 cm. The radius of curvature for the output coupler can therefore change by up to 4%. This will lead to a change in the waist position of 8 cm. This small a change should not appreciably change the mode coupling to the electron beam.

It is possible to calculate analytically the temperature rise in a mirror heated along the center by a Gaussian mode, uniform in the axial coordinate, whose outer edge is uniformly clamped at some temperature.

$$T(\rho) = -\left(\frac{\alpha_B P_l}{4\pi k_{th}}\right)\left[\ln \rho^2 + \lim_{t\to 0}\left(\Gamma(t,(b\rho)^2) - \Gamma(t,b^2)\right)\right] \tag{3}$$

where ρ is the radial location on the mirror normalized to the mirror radius, $\Gamma(t,x)$ is an incomplete Gamma function, $b \equiv \sqrt{2}(\dfrac{a}{\omega_m})$, a is the mirror radius, ω_m is the mode waist size at the mirror, α_B is the bulk absorption, P_1 is the laser power and k_{th} is the mirror thermal conductivity. An approximation to this solution for $r<w_m$ is given by

$$T(\rho) = \left(\frac{\alpha_B P_l}{4\pi k_{th}}\right)\left[\gamma + \ln b^2 - (b\rho)^2 + \frac{(b\rho)^4}{4} - \frac{(b\rho)^6}{18} + \frac{(b\rho)^8}{96} - \frac{(b\rho)^{10}}{600}\right] \tag{4}$$

where the Euler-Mascheroni constant g is equal to 0.577215645. This series approximation is good to better than 1% for $r<w_m$ but for larger radii the series diverges rapidly for any number of terms. The maximum temperature rise will depend on the material properties of the mirror used and logarithmically on the mode waist.

The mirror distortion due to this temperature rise should, to first order, be proportional to the temperature rise. In other words the surface profile should mirror the temperature profile. If this is the case, the mirror distortion should be

$$\delta z(r) \cong \alpha_\epsilon T\left(\frac{r}{a}\right)\frac{h}{2} \tag{5}$$

where α_ϵ is the thermal expansion coefficient of the mirror substrate and h is the thickness of the mirror. This calculated distortion may be expanded in Zernike polynomials [9] to get estimates of the change in the radius of curvature in the mirror and the amplitudes of the spherical aberration terms. Instead of using the radius of the mirror as the reference radius for the Zernike polynomials, we choose to use twice the $1/e$ waist of the optical mode on the mirror. This includes 99.97% of the optical power of a Gaussian mode. When this is done we get the following form for the mirror distortion:

$$\delta z \equiv \frac{P_l}{8\pi F}\left[c_0 + c_1(2\chi^2 - 1) + c_3(6\chi^4 - 6\chi^2 + 1) + c_3(20\chi^6 - 30\chi^4 + 12\chi^2 - 1)\right] \tag{6}$$

where F is a figure of merit for the mirror material which is defined by $F = k_{th}/(h\alpha_\epsilon\alpha)$, and the c_i are the Zernike coefficients of the expansion of equation 3 as a function of $\chi = r/(2w_m)$ multiplied by ($\gamma + \ln b^2$). It is interesting to note that the Zernike coefficients calculated here are independent of the relative size of the mirror and the optical mode. This is due to the fact that the function can be approximated quite well by a polynomial of even orders of c. When the Zernike polynomial fit to this series is done we find the following Zernike coefficients:

c_1	-1.17
c_2	0.44
c_3	-0.17

The fit to the mirror distortion calculated from ANSYS for a Rayleigh range of 37 cm is shown in Figure 2 along with the optical intensity. The Zernike polynomial fit to the distortion is quite good over the range of the optical mode.

From the expansion above, we can show that the change in the Rayleigh range due to the mirror heating is

$$\frac{\Delta z_R}{z_R} \cong \frac{1.17 P_l}{32 F \lambda}\frac{M}{\sqrt{M-1}} . \tag{7}$$
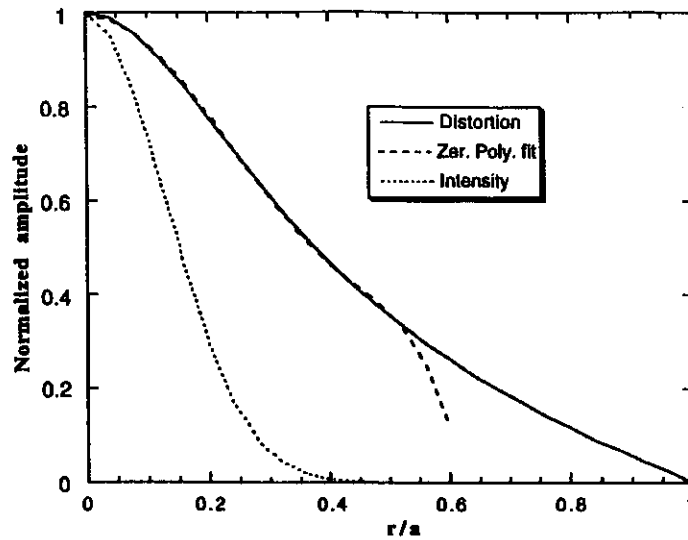
Figure 2. The normalized mirror distortion calculated by ANSYS is plotted along with the intensity of the optical mode and a Zernike polynomial fit including the first three circle polynomials.

We can also compute the spherical aberration terms normalized to the optical wavelength. The maximum aberration amplitude occurs at the mirror center and has an amplitude $\Delta z(0)/\lambda = 0.61 P_l/8\pi F\lambda$. It is instructive to look at the ratio of the aberration measured in waves to the relative change in the Rayleigh range.

$$\frac{\frac{\delta z(0)}{\lambda}}{\frac{\Delta z_R}{z_R}} = 0.664 \frac{\sqrt{M-1}}{M} \tag{8}$$

For large M it is clear that the aberration amplitude will be much less than one wave for even a 100% change in the Rayleigh range but that, even if the radius of curvature is actively controlled, the mirror heating will eventually distort the optical mode more than one fifth of a wave.

Since the mirror substrate must be chosen to be very transparent at the laser wavelength, the thermal properties may not be sufficient to minimize the effects of absorption in the mirror coating. The temperature distribution induced by heating the surface with a Gaussian mode can also be calculated by solving the heat diffusion equation in steady state. The problem in this case is three dimensional and the differential equation becomes

$$\nabla^2 T(\rho) = \frac{2a^2\alpha_s P_l}{M z_R \lambda_c k_{th}} e^{-(b\rho)^2} \delta(\zeta) \tag{9}$$

where T_c is the coating transmission, $\zeta = z/a$ is the dimensionless axial coordinate and α_s is the total absorption in the coating. The solution to this equation is given by the integral

$$T(\rho,\zeta) = \left(\frac{2a^2\alpha_a P_l}{4\pi M z_R \lambda T k_{th}}\right) \int_0^1 \rho' d\rho' \int_0^{2\pi} (\zeta^2 + \rho^2 + \rho'^2 - 2\rho\rho'\cos\phi)^{-1/2} e^{-(b\rho')^2} d\phi \tag{10}$$

Two points may be made about the solution to this equation:

1) The integral of the temperature rise along the axial coordinate z yields the function given in equation (3).

2) Calculation of the mirror distortion due to surface heating using ANSYS indicates that the net distortion from a surface heating is the same as if the mirror were heated uniformly along the axial coordinate.

These two points support the idea of adding the surface heating α_s, scaled by the mirror thickness h and transmission t_c, to the bulk absorption α_B. The change in the Rayleigh range is then given by

$$\frac{\Delta z_R}{z_R} \cong \frac{1.17 P_l}{32 F' \lambda} \frac{M}{\sqrt{M-1}} \quad \text{where } F' = \frac{k_{th}}{(h\alpha_B + \alpha_s(1+1/t_c))\alpha_e} \tag{11}$$

and equation 8 still applies as long as equation 11 is used to calculate the relative change in the Rayleigh range.

The analysis so far does not include the time dependent distortion when the mirror is first heated. It is possible that the aberration and radius of curvature changes during startup may be larger than those shown so far. This can be modeled self-consistently using simulation computer codes such as GLAD [9]. Ultimately one would like to simulate the FEL interaction accurately as well using some code such as FELEX [10]. Simulations using GLAD are described in the next section.

4. MIRROR DISTORTION–NUMERICAL ANALYSIS

4.1 Analytic calculations

If we assume the resonator parameters in Table 2 we can calculate the effect of the mirror distortion using the equations in Section 3. The figure of merit for 6.35 mm thick calcium fluoride, sapphire, and magnesium fluoride mirrors with 0.1% surface absorption is shown in table 3. Using equations (1), (3), (8), and (11) we can calculate the following first order results:

Table 3. Mirror distortion effects for three different mirror materials

	CaF_2	sapphire	MgF_2
Assumed bulk absorption at 3 μm	0.05%	0.1%	0.55%
Figure of merit F' assuming 0.1% surface absorption and 13% transmission.	5.7×10^5	4.5×10^6	1.15×10^6
Temperature rise at mirror center °C	48	17	30
Increase in Rayleigh Range	140%	25%	80%
Shift in mode waist (cm)	20	2.3	9
Max. aberration (waves)	0.14	0.016	0.05

It is obvious that CaF_2 is not an adequate choice. Sapphire is superior both in terms of the effects of mirror heating and radiation damage. MgF_2, is in between the two and seems marginally acceptable.

We can use the new Rayleigh range derived from Table 3 to calculate new resonator parameters which then lead to more heating. This can be done iteratively until a self-consistent solution is found. For CaF_2 the net change in the Rayleigh range is 320%, the net temperature rise is 60 °C and the net change in the mode waist is 87 cm. Assuming the mode remains Gaussian, the transverse scale of the aberration changes but the peak value does not. For this large a change, however, we

cannot assume that the mode remains Gaussian. For sapphire, the net change in the Rayleigh range is 31% and the net temperature rise is 18°C. The net change in the waist position is 3 cm. The net change for MgF₂ is 153% with a waist shift of 23 cm and the temperature rise is 36°C. The self-consistent calculation indicates that MgF₂ is not acceptable but that Sapphire is still fine.

It is worth considering whether this cavity design can scale up to much higher power levels. Note that the scaling of the Rayleigh range change and the aberration amplitude both vary as $P_l / F\lambda$, so increasing the power output and decreasing the wavelength must be compensated by using a material of higher F. Changing the magnification does not help since the aberration amplitude is independent of the mode size. In fact the Rayleigh range will change even more for a larger magnification.

One possible upgrade to the IR Demo would be to increase the electron beam energy to 75 MeV and increase the average current to 6 mA. This would result in over 2 kW of output power. The mode size would be a factor of three smaller and the mirror transmission would be 10%. On the plus side, the optical substrates and coatings available in the 1–1.6 μm wavelength range are extremely low loss. A surface loss of 100 parts per million may be achievable and bulk absorption of 0.05% should be easily achieved. Using sapphire at 1.1 μm, one finds that the figure of merit is 3.1 x 10⁷ and that the warm cavity Rayleigh range would increase by 10% over the cold cavity Rayleigh range, the waist moves 0.9 cm and the temperature rise is only 3 °C. The change in power and wavelength is therefore compensated by the improved absorption properties of sapphire and high quality oxide coatings. We should caution however that the power density in such a cavity would be higher than is generally considered safe and may be susceptible to non-linear absorption. We might therefore require a different design such as the retro-reflecting, re-imaged, ring resonator [12]. Such a design would be required anyway for any power higher than 2 kW.

4.2 Simulations

In order to understand the development of the optical mode as a function of time as the mirror heats, the IR optical cavity was modeled using the commercial geometric optics code GLAD [9]. GLAD correctly models the propagation of the optical mode through an arbitrary series of mirrors, lenses, or apertures. Although the code does not include a FEL gain model, a surrogate gain can be applied over a super-Gaussian region using Beer's law to mimic the FEL interaction.

The local small signal gain is defined as,

$$g(x, y) = g_0 \exp\left[-\left(\frac{x}{X_{rad}}\right)^{2N_x} - \left(\frac{y}{Y_{rad}}\right)^{2N_y} \right] \tag{12}$$

with a local saturated gain,

$$g_{sat}(x, y) = \frac{g(x, y)}{\left[1 + \dfrac{I(x, y)}{I_{sat}}\right]^Q} \tag{13}$$

and local transmission,

$$t(x, y) = \exp[g_{sat}(x, y)z] \tag{14}$$

where the small signal gain $g_0 = 0.08 cm^{-1}$, the supergaussian exponents $N_x = N_y = 2$, the supergaussian radii $X_{rad} = Y_{rad} = 0.03 cm$, the homogeneous saturation exponent $Q = 1$, I(x,y) is the irradiance at (x,y) in $\dfrac{W}{cm^2}$ and the saturation irradiance $I_{sat} = (adjusted value)\dfrac{W}{cm^2}$.

Not included in the gain model is the optical phase shift from the FEL gain but at saturation in the low gain regime that exists in the IR Demo this effect is very small. Another minor shortcoming from this approach is that the details of the saturation characteristics differ between Beer's law and the actual FEL system. Since the FEL gain medium is smaller than the optical mode it is expected that the resulting predictions of the optical mode will be accurate. This has in fact been confirmed by comparison to predictions of other codes.

The code ouputs were compared on a 3 dimensional negative branch unstable resonator [11] where the outcoupling should be extremely sensitive to diffraction effects. Two independent simulations were compared with GLAD. One set of comparisons was run by Ming Xie at Lawrence Berkeley Laboratory (LBL) utilizing the resonator simulation code HOLD, based on the Fox-Li iterative approach[12] with the FEL interaction included by an FEL transfer map[13,14]. The other was done by John Goldstein at Los Alamos National Laboratory (LANL) who developed the computer code FELEX that simulates three-dimensional FEL physics used for analysis and design. Within the wiggler the calculation is based upon the Monte Carlo technique of following the orbits of individual electrons, and then evaluating the macroscopic current to determine the interaction with the optical field [8,10].

The GLAD FEL model was run for optical cavity magnifications of M=1.062, M=1.1, and M=1.15. The results are summarized in Fig. 3. Also shown are results, at some of the same magnification values, of the LBL and LANL cavity models.
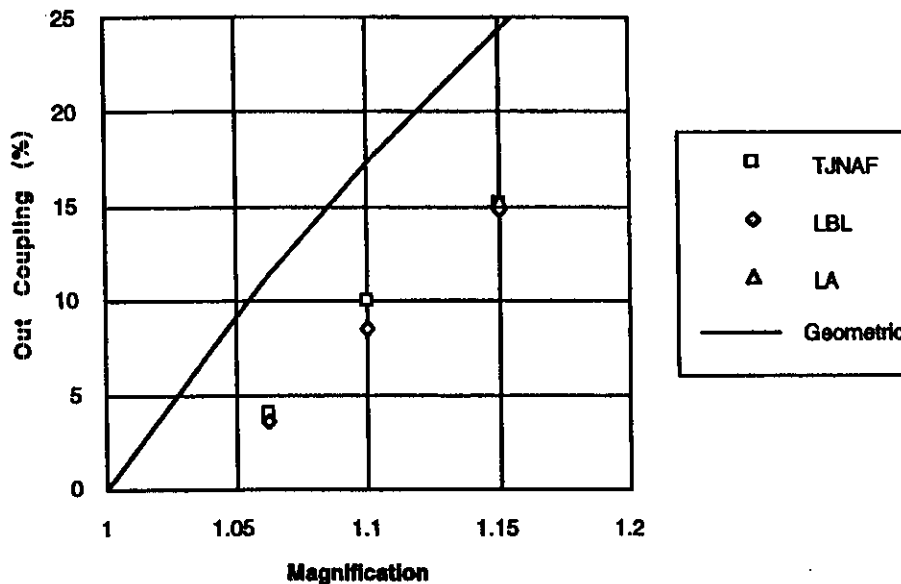

Figure 3. FEL output coupling comparison, wiggler bore radius = 5.0 mm

As can be seen from the graph in Fig. 3, the GLAD model performed within the geometric output coupling of

$$OC_{max} = 1 - \frac{1}{M^2} \tag{15}$$

and agreed within 2% with the LBL and LANL models at M = 1.15, 18% with the LBL model at M = 1.1, and 11% with the LBL model at M = 1.062. Other cases where strong diffraction occurred in the wiggler region did not show such good agreement. Results on occasion differed by 50%.

Despite these shortcomings, the model does allow for a reasonable prediction of the diffraction losses in the cavity in the IR Demo case, the mode profile both in the FEL and on the mirrors, the Strehl ratio of the outcoupled beam, and, most importantly, it permits an investigation of the system's stability against perturbations due to thermal effects.

The thermal distortion perturbations might proceed as follows: when the mirror fluence begins to heat the outcoupling mirror due to the transmitted power, the primary effect is an increase in the focal length. This causes the optical mode on the mirror to become smaller on subsequent passes. The tighter mode then leads to increased distortion over the smaller area. The fundamental question is whether this process leads to a stable solution or the FEL goes into a relaxation oscillation as the mode tightens until the FEL no longer can operate, the FEL shuts down, and the process begins anew.

In the GLAD code FEL model the gain region was set as 115 cm long in the center of the cavity. Elliptical apertures of 0.5 by 1.5 cm radius were put at the end of the wiggler to approximate the diffraction effects of the wiggler vacuum tube. The resonator geometry was as specified in table 4. Only the distortion in the outcoupler was considered in these studies.

The outcoupler was assumed to transmit 13% of the incident power and absorb 0.1%/cm through the 0.635 cm of its thickness. Coating and surface absorption were ignored in this initial calculation although they can potentially be of significance because of the high intracavity power. The case run is equivalent to a figure of merit of 8.1 x 10^6 in table 3. As shown in the previous section the results can be scaled to other wavelengths, powers, and coating and bulk absorptions according to $P_i / F\lambda$.

The mirror was assumed to be cooled on its edges to ambient temperature. Materials properties of CaF_2 were used in calculating the temperature drop and distortion. The saturation power of the Beer's law formula was arbitrarily set to a value that produced 1 kW of outcoupled power.

Thermal effects can be modeled in GLAD by the use of an impulse function approach. That is, a delta function heat source in the center of a cylindrically symmetric plate will spread as a function of time (t) according to a Gaussian heat distribution (the impulse function) satisfying the thermal diffusion equation.

$$Q(r,t) = \frac{Qe^{\frac{-r^2 \rho C}{4 k_{th} t}}}{4\pi h k_{th} t}$$

(16)

where ρ is the density, C is the heat capacity, k_{th} is the thermal conductivity, and h is the material thickness.

The optical mode is initially launched from a simple Gaussian mode in the center of the FEL cavity. At each pass, when the mode hits the outcoupler mirror a thermal distribution array is produced proportional to the local fluence. This is convolved with the thermal Gaussian impulse response and then added to the previous heat array. Any heat lying outside the outer radius of the mirror is clipped and assumed lost. The local heat deposited is translated into a temperature by the CaF_2 heat capacity and that leads to a face distortion on the mirror according to the coefficient of expansion of the local temperature over one half the thickness of the mirror (it expands equally in both directions). This produces a phase front distortion on the optical wave which is propagated through the cavity for the next pass. The process continues until a steady state is attained.

One difficulty in modeling the system is the long time scale required to reach steady state. This requires many iteration steps for convergence, resulting in long computation times. As a work-around for this difficulty, the system was scaled by increasing both the optical power in the cavity and the thermal conductivity of the substrate. The optical mode produced is identical and the effective time scale can be increased by a factor of 50 for a proportional reduction in computation time.

Figure 4-a, b, c, d shows the temperature profile on the outcoupler at t = 0.77, 2.3, 3.08, and 6.15 sec. A scan of the intensity and phase at the outcoupler and the mode shape entering the wiggler for t=6.15 sec are shown in Figure 5. The peak temperature rise in the center of the mirror is 4.4 °C, 20% more than predicted by the analytic approach. There is a corresponding increase in the peak distortion. Nonetheless the mode comes to a stable operating point with modes that are close to Gaussian. The saturated mode in the center of the wiggler is shown in Figure 6 to appear nearly an ideal Gaussian.
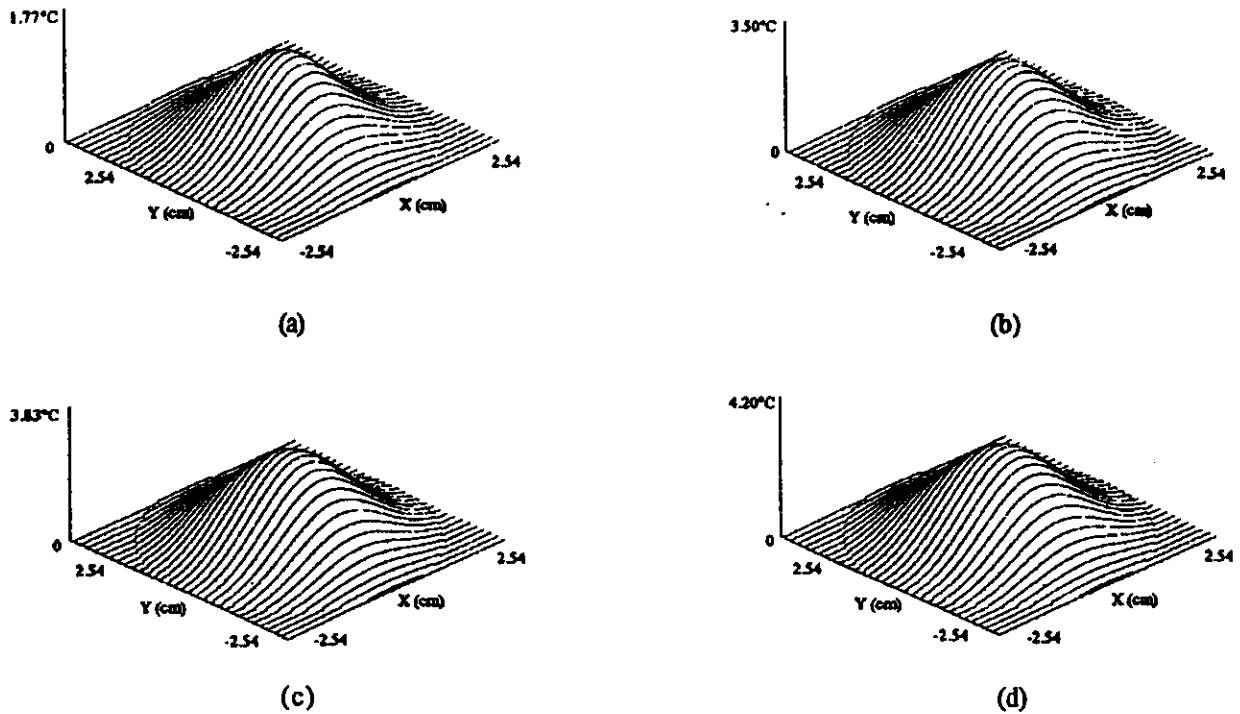
Figure 4. Temperature profile on the outcoupler at 4 different times after initiation of lasing. a) 0.77 sec, b) 2.3 sec, c) 3.08 sec, d) 6.15 sec.
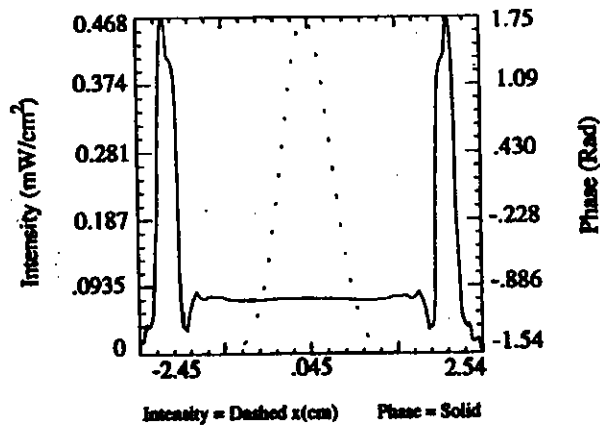

Figure 5. Intensity and phase of the beam at the output coupler at saturation.

This leads us to believe that deleterious effects on the FEL power should be minimal and the model confirms that the predicted saturation power does not change significantly. The outcoupled mode is essentially diffraction limited with a Strehl of > 0.9. The primary effect of the distortion is a slight change in the radius of curvature in the outcoupled wave. This will be compensated in the real system by moving a collimating mirror by 5 cm as the FEL operating point stabilizes in power. The model confirms predictions that the system comes to a stable operating point over a real time period of tens of seconds. Negative effects on the overall performance of the FEL are minimal from this level of distortion.